Inorganic Chemistry
Article

Inorg. Chem. **2010**, *49*, 5723–5736 **5723**
DOI: 10.1021/ic100667f

Insights into the Origin of Cooperative Effects in the Spin Transition of $[Fe(NH_2trz)_3](NO_3)_2$: the Role of Supramolecular Interactions Evidenced in the Crystal Structure of $[Cu(NH_2trz)_3](NO_3)_2 \cdot H_2O$

Marinela M. Dîrtu,[†] Christine Neuhausen,[‡] Anil D. Naik,[†] Aurelian Rotaru,[§] Leonard Spinu,[§,∥] and Yann Garcia*[,†]

[†]*Institut de la Matière Condensée et des Nanosciences, Université Catholique de Louvain, Place L. Pasteur 1, 1348 Louvain-la-Neuve, Belgium,* [‡]*Ecole Polytechnique Fédérale de Lausanne, Institut de physique des systèmes biologiques, Bât. Sciences Physiques UNIL, Lausanne, 1015, Switzerland,* [§]*Advanced Materials Research Institute, and* [∥]*Department of Physics, University of New Orleans, New Orleans, Louisiana 70148*

Received April 8, 2010

The thermally induced hysteretic spin transition (ST) that occurs in the polymeric chain compound $[Fe(NH_2trz)_3](NO_3)_2$ (**1**) above room temperature ($T_c^{\uparrow}$ = 347 K, $T_c^{\downarrow}$ = 314 K) has been tracked by ^{57}Fe Mössbauer spectroscopy, SQUID magnetometry, differential scanning calorimetry (DSC), and X-ray powder diffraction (XPRD) at variable temperatures. From the XRPD pattern indexation, an orthorhombic primitive cell was observed with the following cell parameters: a = 11.83(2) Å, b = 9.72(1) Å, c = 6.361(9) Å at 298 K (low-spin state) and a = 14.37(2) Å, b = 9.61(4) Å, c = 6.76(4) Å at 380 K (high-spin state). The enthalpy and entropy variation associated to the ST of **1**, have been evaluated by DSC as ΔH = 23(1) kJ mol^{-1} and ΔS = 69.6(1) J mol^{-1} K^{-1}. These thermodynamic data were used within a two-level Ising like model for the statistical analysis of First Order Reversal Curve (FORC) diagram that was recorded for **1**, in the cooling mode. Strong intramolecular cooperative effects are witnessed by the derived interaction parameter of J = 496 K. The crystal structure of $[Cu(NH_2trz)_3](NO_3)_2 \cdot H_2O$ (**2**) was obtained thanks to high quality single crystals prepared by slow evaporation after hydrothermal pretreatment. The catena poly[μ-tris(4-amino-1,2,4-triazole-*N1,N2*) copper(II)] dinitrate monohydrate (**2**) crystallizes in the monoclinic space group *C*2/*c*, with a = 16.635(6) Å, b = 13.223(4) Å, c = 7.805(3) Å, β = 102.56(3)°, Z = 4. Complex **2** is a 1D infinite chain containing triple *N1,N2*-1,2,4-triazole bridges with an intra-chain distance of Cu···Cu = 3.903(1) Å. A dense H-bonding network with the nitrate counteranion involved in intra-chain and inter-chain interactions is observed. Such a supramolecular network could be at the origin of the unusually large hysteresis loop displayed by **1** ($\Delta T \sim 33$ K), as a result of an efficient propagation of elastic interactions through the network. This hypothesis is strengthened by the crystal structure of **2** and by the absence of crystallographic phase transition for **1** over the whole temperature range of investigation as shown by XRPD.

1. Introduction

A growing interest in the coordination chemistry of 4-substituted-1,2,4-triazole derivatives has been accentuated while searching for crystal structure-magnetic properties relationships for 3d transition metal complexes with these ligands.[1] Indeed, such bidentate molecules are able to propagate elastic[2] and magnetic interactions[3] between transition metal ions in polynuclear complexes, which are of fundamental importance in molecular magnetism.[4] In particular, several one-dimensional (1D) spin crossover (SCO) chains of formula $[Fe(4\text{-}R\text{-}1,2,4\text{-triazole})_3](anion)_2$ have been prepared and thoroughly investigated.[5] These coordination polymers generally display in the solid state a spin transition (ST) with a hysteresis width of variable extent, sometimes centered near room temperature.[2,5,6] Their associated thermochromism make them potentially useful for various applications such

*To whom correspondence should be addressed. E-mail: yann.garcia@uclouvain.be.

(1) (a) Haasnoot, J. G. *Coord. Chem. Rev.* **2000**, *131*, 200. (b) Beckmann, U.; Brooker, S. *Coord. Chem. Rev.* **2003**, *245*, 17. (c) Kitchen, J. A.; Brooker, S. *Coord. Chem. Rev.* **2008**, *252*, 2072.

(2) Kahn, O.; Codjovi, E.; Garcia, Y.; van Koningsbruggen, P. J.; Lapouyade, R.; Sommier, L. In *Molecule-Based Magnetic Materials*; Turnbull, M. M., Sugimoto, T., Thompson, L. K., Eds.; ACS Symposium Series 644; American Chemical Society: Washington, DC, 1996, 298.

(3) (a) Garcia, Y.; van Koningsbruggen, P. J.; Bravic, G.; Guionneau, P.; Chasseau, D.; Cascarano, G. L.; Moscovici, J.; Lambert, K.; Michalowicz, A.; Kahn, O. *Inorg. Chem.* **1997**, *36*, 6357. (b) Garcia, Y.; van Koningsbruggen, P. J.; Bravic, G.; Chasseau, D.; Kahn, O. *Eur. J. Inorg. Chem.* **2003**, 356.

(4) (a) Kahn, O. *Molecular Magnetism*; Wiley-VCH: New York, 1993. (b) *Magnetism: Molecules to Materials I*−*V*; Miller, J. S., Drillon, M., Eds.; Wiley VCH: Weinheim, 2001−2004.

(5) Garcia, Y.; Niel, V.; Muñoz, M. C.; Real, J. A. *Top. Curr. Chem.* **2004**, *233*, 229.

Published on Web 05/27/2010

as display and memory devices units,[7] sensors,[8] and cold channel control units in food and medicals storage.[9]

The origin of the hysteresis loop of these materials and its thermal extent are not yet fully understood.[10] It is recognized that strengthening of intramolecular interactions by triply 1,2,4-triazole bridges connecting spin changing molecules can promote cooperative effects, resulting in the observation of hysteresis width ranging between 2 and 20 K.[5] Indeed, 1D chains where the Fe^{II} ions are linked by loose bridges all display gradual SCO behavior without any hysteresis effect. This is the case when triply bis-tetrazoles bridges with flexible spacers are employed[11] or when single bridges are used (e.g., 1,2-bis(4-pyridyl)etha(e)ne,[12] 4,4′-bipyridine,[13] dicyanamide[14]). Intermolecular interactions are believed to also contribute to the ST cooperative mechanism, thus resulting in larger hysteresis loops.[2,15,16] There indeed exist three examples of 1D chains where intermolecular interactions in combination with the above-mentioned intramolecular interactions may contribute to the effective propagation of elastic interactions between spin changing molecules. This is the case for $[Fe(Htrz)_2trz]BF_4$ (Htrz = 4-*H*-1,2,4-triazole, trz = triazolato) that displays a ST above room temperature with a hysteresis width of ∼40 K,[15] and for $[Fe(hyptrz)_3](4\text{-chloro-3-nitrophenylsulfonate})_2 \cdot H_2O$ (hyptrz = 4-(3′-hydroxypropyl)-1,2,4-triazole) that display a ST with an hysteresis width of ∼50 K below room temperature.[16] For the first case, the BF_4^- anion directly bridges neighboring chains through hydrogen bonding as deduced from WAXS experiments.[17] For the second case, $\pi-\pi$ stacking interactions of the anions as well as direct hydrogen bonding between the 4-R substituent of neighboring chains were observed in the analogous Cu^{II} crystal structure of the 1D chain.[17] The third example concerns $[Fe(NH_2trz)_3](NO_3)_2$ (NH_2trz = 4-amino-1,2,4-triazole) (**1**) whose large hysteresis of ∼35 K,[2,18] could originate from intermolecular interactions involving the nitrate as concluded from muon spin relaxation (μSR) experiments.[19]

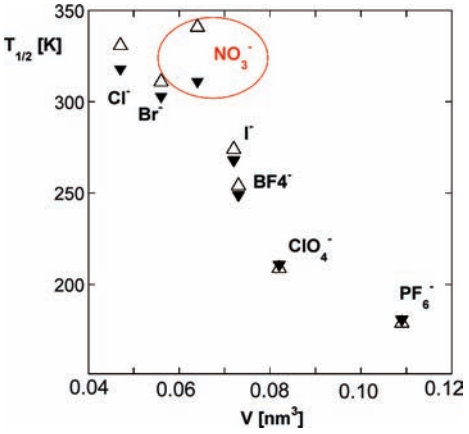

Figure 1. Variation of transition temperature, $T_{1/2}$, as deduced from Mössbauer spectroscopy, on cooling (▼) and warming modes (Δ) versus the anion volume for $[Fe(NH_2trz)_3](anion)_2$.[20b] The circle highlights the wider hysteresis width of the nitrate derivative.

It is however known that the ST regime of $[Fe(NH_2trz)_3](anion)_2$ chain compounds can be tuned over a wide thermal domain by modifying the nature of the non-coordinated anion in the crystal lattice.[5] This conclusion was supported by a useful anion database for these materials including monovalent inorganic anions (Cl^-, BF_4^-, ClO_4^-, PF_6^-, ...) and doubly charged fluoride anions (SnF_6^{2-}, ZrF_6^{2-}, GeF_6^{2-}, ...).[20] This comprehensive work confirmed a linear relationship between the transition temperatures, $T_{1/2}^{\downarrow}$ on cooling and $T_{1/2}^{\uparrow}$ on warming, and the anion volume for monovalent anions (Figure 1). Indeed, when the volume of the anion decreases, the transition temperature increases and the covalency of the Fe−N bonds within the chain increases.[21] Interestingly, the transition temperatures of **1** are located well above the linear regime (Figure 1) despite the monovalent character of the nitrate anion. In addition, the hysteresis width of **1** is much wider than the one usually observed for these ST materials.[5] This difference in properties may originate from the planar nature of the nitrate anion, compared to the spherical geometry of the other inserted monovalent anions, which would allow the propagation of elastic interactions in a directional manner between chains, thanks to hydrogen bonding.

This hypothesis was probed by preparing novel $Fe^{II}-NH_2trz$ chain compounds including anions having planar aromatic rings (benzene sulfonate,[22] naphthalene sulfonate derivatives[23]) which can eventually promote $\pi-\pi$ interactions. However, the hysteresis width of such ST materials did not exceed 20 K.[5] Thus, it can be concluded that the use of planar aromatic anions is not a sufficient

(6) (a) Kröber, J.; Codjovi, E.; Kahn, O.; Grolière, F.; Jay, C. *J. Am. Chem. Soc.* **1993**, *115*, 9810. (b) Bronisz, R.; Drabent, K.; Polomka, P.; Rudolf, M. *Conf. Proc. ICAME1995* **1996**, *2*, 11. (c) Yokoyama, T.; Murakami, Y.; Kiguchi, M.; Komatsu, T.; Kojima, N. *Phys. Rev. B* **1998**, *58*, 14238. (d) Garcia, Y.; van Koningsbruggen, P. J.; Lapouyade, R.; Rabardel, L.; Kahn, O.; Wieczorek, M.; Bronisz, R.; Ciunik, Z.; Rudolf, M. F. *C. R. Acad. Sci.* **1998**, *IIc*, 523. (e) Dîrtu, M. M.; Naik, A. D.; Marchand-Brynaert, J.; Garcia, Y. *J. Phys. Conf. Ser.* **2010**, *217*, 012085.
(7) (a) Kahn, O.; Kröber, J.; Jay, C. *Adv. Mater.* **1992**, *4*, 718. (b) Kahn, O.; Jay-Martinez, C. *Science* **1998**, *279*, 44.
(8) Garcia, Y.; Ksenofontov, V.; Gütlich, P. *Hyperfine Interact.* **2002**, *139/140*, 543.
(9) Garcia, Y.; Ksenofontov, V.; Mentior, S.; Dîrtu, M. M.; Gieck, C.; Bhatthacharjee, A.; Gütlich, P. *Chem.—Eur. J.* **2008**, *14*, 3745.
(10) Murray, K. S.; Kepert, C. P. *Top. Curr. Chem.* **2004**, *233*, 195.
(11) van Koningsbruggen, P. J.; Garcia, Y.; Kahn, O.; Fournès, L.; Kooijman, H.; Spek, A. L.; Haasnoot, J. G.; Moscovici, J.; Provost, K.; Michalowicz, A.; Renz, F.; Gütlich, P. *Inorg. Chem.* **2000**, *39*, 1891.
(12) Matouzenko, G. S.; Perrin, M.; le Guennic, B.; Genre, C.; Molnar, G.; Bousseksou, A.; Borshch, S. A. *Dalton Trans.* **2007**, *9*, 934.
(13) (a) Matouzenko, G. S.; Molnar, G.; Brefuel, N.; Perrin, M.; Bousseksou, A.; Borshch, S. A. *Chem. Mater.* **2003**, *15*, 550. (b) Genre, C.; Matouzenko, G. S.; Jeanneau, E.; Luneau, D. *New J. Chem.* **2006**, *30*, 1669.
(14) Genre, C.; Jeanneau, E.; Bousseksou, A.; Luneau, D.; Borshch, S. A.; Matouzenko, G. S. *Chem.—Eur. J.* **2008**, *14*, 697.
(15) Kröber, J.; Audière, J.-P.; Claude, R.; Codjovi, E.; Kahn, O.; Haasnoot, J. G.; Grolière, F.; Jay, C.; Bousseksou, A.; Linares, J.; Varret, F.; Gonthier-Vassal, A. *Chem. Mater.* **1994**, *6*, 1404.
(16) Garcia, Y.; Moscovici, J.; Michalowicz, A.; Ksenofontov, V.; Levchenko, G.; Bravic, G.; Chasseau, D.; Gütlich, P. *Chem.—Eur. J.* **2002**, *8*, 4992.
(17) Verelst, M.; Sommier, L.; Lecante, P.; Mosset, A.; Kahn, O. *Chem. Mater.* **1998**, *10*, 980.
(18) Lavrenova, L. G.; Ikorskii, V. N.; Varnek, V. A.; Oglezneva, I. M.; Larionov, S. V. *Koord. Khim.* **1986**, *12*, 207.
(19) Garcia, Y.; Campbell, S. J.; Lord, J. S.; Boland, Y.; Ksenofontov, V.; Gütlich, P. *J. Phys. Chem. B* **2007**, *111*, 11111.
(20) (a) Dîrtu, M. M.; Garcia, Y.; Nica, M.; Rotaru, A.; Linares, J.; Varret, F. *Polyhedron* **2007**, *26*, 2259. (b) Dîrtu, M. M.; Rotaru, A.; Gillard, D.; Linares, J.; Codjovi, E.; Tinant, B.; Garcia, Y. *Inorg. Chem.* **2009**, *48*, 7838.
(21) Varnek, V. A.; Lavrenova, L. G. *J. Struct. Chem.* **1995**, *36*, 104.
(22) (a) Codjovi, E.; Sommier, L.; Kahn, O. *New. J. Chem.* **1996**, *20*, 503. (b) Toyazaki, S.; Murakami, Y.; Komatsu, T.; Kojima, N.; Yokoyama *Mol. Cryst. Liq. Cryst.* **2000**, *343*, 175. (c) Toyazaki, S.; Nakanishi, M.; Komatsu, T.; Kojima, N.; Matsumura, D.; Yokoyama, T. *Synth. Met.* **2001**, *121*, 1794.
(23) van Koningsbruggen, P. J.; Garcia, Y.; Codjovi, E.; Lapouyade, R.; Kahn, O.; Fournès, L.; Rabardel, L. *J. Mater. Chem.* **1997**, *7*, 2069.

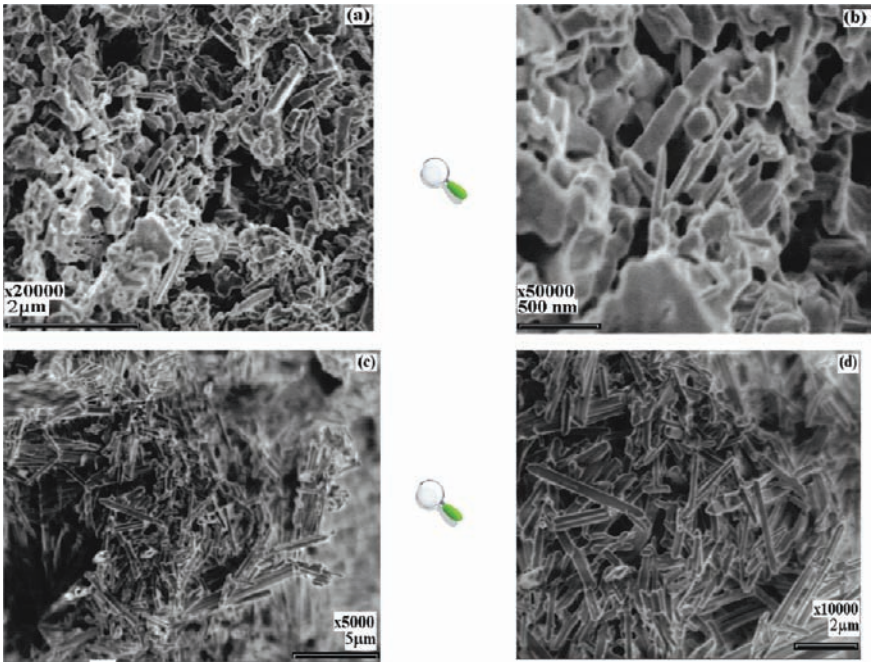

Figure 2. SEM images of powders at different resolutions of $[Fe(NH_2trz)_3](NO_3)_2$, **1**, (a), (b), and of $[Cu(NH_2trz)_3](NO_3)_2 \cdot H_2O$, **2**, (c), (d).

condition to observe a wide hysteresis loop. In the absence of crystal structure of a 1D $Fe^{II}-NH_2trz$ chain containing the nitrate anion, it was difficult to draw further conclusions. These materials indeed hardly crystallize, and only a few Cu^{II} analogues were obtained by slow evaporation of the reaction medium or by recrystallization of the powders of the target compounds.[3,16,20b,24] In this context, recrystallization of powders of $[Cu(NH_2trz)_3](NO_3)_2 \cdot H_2O$ (**2**) after hydrothermal treatment afforded single crystals that were analyzed in this work by single crystal X-ray diffraction. The crystal structure reveals 1D triple bridged *N1*,*N2*-1,2,4-triazole Cu^{II} chains and allows the study of the supramolecular organization of the anion with respect to other components of the system. To get deeper insights to the origin of cooperative effects of the ST of **1**, First-Order Reversal Curves (FORC) were recorded along with superconductiong quantum interference device (SQUID) measurements. This study was completed by differential scanning calorimetry (DSC) and variable temperature X-ray powder diffraction and ^{57}Fe Mössbauer spectroscopy carried out above 293 K where the ST proceeds.

2. Results

2.1. Synthesis. 1 was precipitated as a pink powder containing nanorods (length ~300−800 nm and thickness ~66 nm) that were identified by scanning electronic microscopy (SEM) (Figure 2a, b).

Attempts to obtain single crystals of **1** by slow evaporation, slow diffusion, recrystallization, and hydrothermal methods, all failed. The X-ray powder diffraction pattern (Figure 3) indicates a rather crystalline material which is similar to the one displayed by **2**. Repeated attempts to grow single crystals of **2** by slow evaporation, from an aqueous solution of the reaction medium at room temperature afforded dendrite type crystals. Recrystallization of a powder of **2** afforded a microcrystalline powder that provided a well resolved X-ray diffractogram (Figure 3), but no single crystals suitable for a X-ray analysis. The high crystalline morphology of this sample was confirmed by SEM with elongated rods of 120−330 nm length (Figure 2c,d). These features prompted us to invest more efforts in the recrystallization process. The powder of **2** was then dissolved in distilled water and treated hydrothermally in an acid digestion bond at 155 °C for 36 h. After cooling to room temperature, slow evaporation of the solution afforded after 1 week thin needles that are isostructural to the powder of **2**, as deduced from X-ray powder diffraction (Figure 3) and suitable for a single crystal X-ray diffraction analysis (Section 2.2.). A thermogravimetric measurement was carried out for **2** over the temperature range 25−900 °C. The residue obtained after ~900 °C was identified as CuO by comparison of its X-ray powder diffractogram with the JPCDS-JCDD database. This allowed us to derive the Cu % from the TGA analysis which is in agreement with

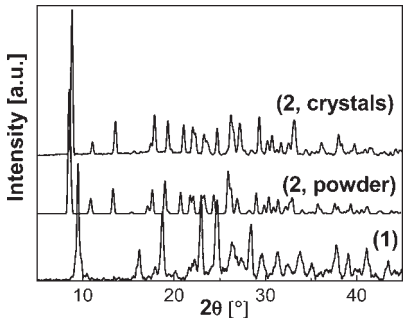

Figure 3. X-ray powder diffraction patterns at 293 K for **1** and **2**.

(24) (a) Sinditskii, V. P.; Sokol, V. I.; Fogel'zang, A. E.; Dutov, M. D.; Serushkin, V. V.; Porai-Koshits, M. A.; Svetlov, B. S. *Russ. J. Inorg. Chem.* **1987**, *32*, 1586. (b) Drabent, K.; Ciunik, Z. *Chem. Commun.* **2001**, *14*, 1254. (c) Seredyuk, M.; Gaspar, A. B.; Muñoz, M. C.; Verdaguer, M.; Villain, F.; Gütlich, P. *Eur. J. Inorg. Chem.* **2007**, 4481. (d) Seredyuk, M.; Gaspar, A. B.; Ksenofontov, V.; Galyametdinov, Y.; Verdaguer, M.; Villain, F.; Gütlich, P G. *Inorg. Chem.* **2008**, *47*, 10232.

Table 1. Crystallographic Data and Structure Refinements for $[Cu(NH_2trz)_3](NO_3)_2 \cdot H_2O$ (**2**) at 293(2) K

empirical formula	$C_6\ H_{13}\ Cu\ N_{14}\ O_7$
M (g/mol)	456.84
crystal system	monoclinic
space group	C 2/c (n°15)
a/Å	16.635(6)
b/Å	13.223(4)
c/Å	7.805(3)
β/deg	102.56(3)°
V/Å^3	1675.7(10)
Z	4
D/g.cm^{-3}	1.811
crystal size (mm)	0.1 × 0.1 × 0.9
F(000)	928
reflections collected	873
independent reflections	873
no. parameters	149
goodness of fit on F^2	1.076
R1, wR2 [$I > 2\sigma(I)$]	0.0534, 0.1423
R1, wR2 [all data]	0.0614, 0.1510
largest difference peak and hole/e Å^{-3}	0.986 and −0.631 e Å^{-3}

the expected one for **2**. The crystals and powder of **2** have identical IR spectra. The bands assigned to ring torsion of triazole (619 cm^{-1}) and the N−N stretching bands (1197 cm^{-1}) are shifted to 621 cm^{-1} and 1218 cm^{-1}, respectively, thus confirming the coordination of Cu^{II} to the triazole ring.[24a] The strong band $\nu_3 \sim 1384$ cm^{-1} and the weak band $\nu_2 \sim 827$ cm^{-1} are characteristic of the asymmetric stretch and out-of-plane bend of nitrate anion,[25] thus confirming the presence of a non-coordinated counteranion. Diffuse reflectance spectra of **2** as powder or crystals show a broad asymmetric band in the range 440−870 nm which is due to a d-d transition, with a maximum at 15385 cm^{-1}, which is in agreement with the presence of a CuN_6 chromophore and a tetragonal distortion of Cu^{II} octahedra.[26]

2.2. X-ray Crystal Structure of $[Cu(NH_2trz)_3](NO_3)_2 \cdot H_2O$ (2). $[Cu(NH_2trz)_3](NO_3)_2 \cdot H_2O$ (**2**) crystallizes in the monoclinic system (*C*2/*c*). The crystallographic data are presented in Table 1, and selected bond lengths and angles are given in Table 2a. Each Cu^{II} ion is coordinated to six N atoms belonging to six NH_2trz ligands setting up an octahedral symmetry, as indicated by the bond lengths and angles involving Cu^{II} (Table 2a). The basal plane of the octahedra is formed by four nitrogen donor atoms at 1.991(4) Å and 2.081(4) Å and two NH_2trz ligands that coordinate axially at 2.372(4) Å. The axial bond lengths are larger than the equatorial ones because of the Jahn−Teller effect. These Cu−N bond lengths are shorter than for other Cu^{II} 1D chain with NH_2trz including other anions (Table 3). The bidentate NH_2trz ligand bridges the copper ions through the *N1*- and *N2*- nitrogen atoms to form a 1D infinite polymer (Figure 4). Compared to other crystallized Cu^{II} 1D chain compounds, only one repeating Cu^{II} type has been found within the chain, the octahedron thus appears to be less distorted (distortion parameter[27] $\sum = 13.0(5)°$) (Table 3).

The Cu^{II} octahedra are oriented in an *ababa* arrangement within a chain (Figure 4). The intra-chain distance

Table 2. (a) Selected Bond Distances (Å) and Angles (deg), and (b) Inter-Atomic Distances and Angles (deg) for Hydrogen Bond Interactions in $[Cu(NH_2trz)_3](NO_3)_2 \cdot H_2O$ (**2**)

(a) Bond Distances and Angles

bond	length	bond	angle
Cu1−N3	2.372(4)	N4−Cu1−N4	180.0(4)
Cu1−N4	1.991(4)	N4−Cu1−N7	90.53(17)
Cu1−N7	2.081(4)	N4−Cu1−N7	89.47(17)
N3−N4	1.391(5)	N7−Cu1−N7	180.0(3)
N4−C2	1.300(8)	N4−Cu1−N3	89.88(17)
N5−N6	1.402(10)	N4−Cu1−N3	90.12(17)
N6−C3	1.344(7)	N7−Cu1−N3	87.10(16)
N7−C3	1.305(7)	N7−Cu1−N3	92.60(16)
N7−N7	1.385(8)	N3−Cu1−N3	180.0(3)
N8−O1	1.204(9)	C2−N2−C1	105.5(5)
N8−O2	1.195(12)	C2−N2−N1	128.1(5)
N8−O3	1.225(10)	C1−N3−N4	126.2(5)
		C1−N3−N4	106.0(4)
		C1−N3−Cu1	128.1(4)
		N4−N3−Cu1	125.4(3)
		C2−N4−N3	107.0(5)
		C2−N4−Cu1	128.3(4)
		N3−N4−Cu1	124.4(3)
		N3−C1−N2	111.2(5)
		N4−C2−N2	110.2(5)
		C3−N6−C3	105.3(7)
		C3−N6−N5	127.4(4)
		C3−N6−N5	127.4(4)
		C3−N7−N7	106.7(3)
		C3−N7−Cu1	126.0(4)
		N7−N7−Cu1	126.81(13)
		N7−C3−N6	110.6(6)
		O2−N8−O1	118.4(10)
		O2−N8−O3	122.3(11)
		O1−N8−O3	119.2(11)

(b) Inter-Atomic Distances and Angles

D−H	D−H	H···A	∠D−H−A	D···A	A
N5−H5A	*0.86*	*3.023*	*89*	*3.126*	*O1* [*−0.5+x, 0.5−y, −0.5+z*]
N5−H5A	*0.86*	*3.023*	*89*	*3.126*	*O1* [*0.5−x, 0.5−y, 1−z*]
N1−H1A	*0.86*	*3.102*	*90*	*3.224*	*O3* [*0.5−x, 0.5−y, −z*]
N5−H5A	*0.86*	*2.720*	*125*	*3.229*	*O2* [*0.5−x, 0.5+y, 0.5−z*]
N5−H5A	*0.86*	*2.720*	*119*	*3.229*	*O2* [*−0.5+x, 0.5+y, z*]
C2−H2	*1.01*	*2.974*	*87*	*3.087*	*O1* [*0.5−x, 0.5−y, −z*]
C3−H3	*0.90*	*2.963*	*87*	*3.048*	*O1* [*−0.5+x, 0.5−y, −0.5+z*]
N1−H1A	*0.86*	*2.312*	*165*	*3.151*	*O1* [*x, y, −1+z*]
N1−H1A	*0.86*	*3.129*	*84*	*3.159*	*O2* [*x, −y, −0.5+z*]
C1−H1	*1.01*	*2.248*	*157*	*3.125*	*O3* [*x, y, z*]
C2−H2	*1.01*	*2.151*	*163*	*3.129*	*O3*[*x, y, −1+z*]
C3−H3	*0.90*	*2.350*	*162*	*3.215*	*O4* [*0.5−x, 0.5−y, −z*]
O4−H4	*0.78*	*2.648*	*149*	*3.339*	*O1* [*1−x, y, 0.5−z*]
O4−H4	*0.78*	*2.312*	*137*	*2.931*	*O2* [*1−x, y, 0.5−z*]

Cu···Cu = 3.903(1) Å, is in the expected range for 1D Cu^{II} coordination polymers with 1,2,4-triazole ligands. This value varies depending on the counteranion and the number of Cu^{II} types within a chain (Table 3). This distance is, however, higher than for the Fe^{II} derivatives, with a Fe···Fe ∼ 3.5 Å as deduced by EXAFS measurements.[28] For **2**, the inter-chain distance Cu···Cu distance

(25) Nakamoto, K. *Infrared and Raman Spectra of Inorganic and coordination Compounds*, 5 ed., Part B; Wiley-Interscience: New York, 1997.
(26) Hathaway, B. J.; Billing, D. E. *Coord. Chem. Rev.* **1970**, *5*, 143.
(27) Marchivie, M.; Guionneau, P.; Letard, J. F.; Chasseau, D. *Acta Crystallogr.* **2005**, *B61*, 25.

(28) (a) Michalowicz, A.; Moscovici, J.; Ducourant, B.; Cracco, D.; Kahn, O. *Chem. Mater.* **1995**, *7*, 1833. (b) Michalowicz, A.; Moscovici, J.; Kahn, O. *J. Phys. IV* **1997**, *7*, 633.

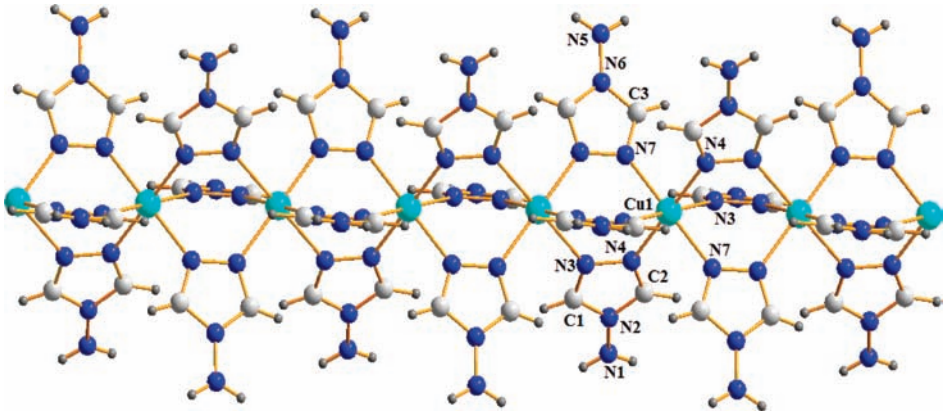

Figure 4. 1D chain of $[Cu(NH_2trz)_3](NO_3)_2 \cdot H_2O$ running along the *c* axis illustrating the atomic labeling scheme (counteranions have been omitted for clarity).

Table 3. Collection of Crystallographic Data for the $[Cu(NH_2trz)_3]$anion$\cdot n H_2O$ Chain Complexes

anion	*n*	bond distances (Å)	octahedra sequence	crystal system, space group	octahedral distortion ($\sum$)	ref.
BF_4^-	1	Cu···Cu = 3.922 Cu1−N11 = 2.379 Cu2−N12 = 1.977 Cu1−N21 = 2.003 Cu2−N22 = 2.423 Cu1−N31 = 2.067 Cu2−N32 = 2.059	ab ab ab	triclinic/$P\bar{1}$	$\sum_{(Cu1)}$ = 12.68(5)° $\sum_{(Cu2)}$ = 22.20(5)°	24b
ClO_4^-	1/3	Cu−N = 2.01−2.11 (eq. plane) Cu−N = 2.26−2.38 (axial plane)		triclinic/$P\bar{1}$		24a
$BF_4^-/(SiF_6^{-2})_{0.5}$	2	Cu···Cu = 3.877, 3.886 Cu1−N11 = 2.426 Cu2−N12 = 2.017 Cu1−N21 = 2.018 Cu2−N22 = 2.327 Cu1−N31 = 2.040 Cu2−N32 = 2.042 Cu3−N41 = 2.315 Cu2−N42 = 2.018 Cu3−N51 = 2.013 Cu2−N52 = 2.369 Cu3−N61 = 2.096 Cu2−N62 = 2.037	ab ab ab	triclinic/$P\bar{1}$	$\sum_{(Cu1)}$ = 21.92(5)° $\sum_{(Cu2)}$ = 14.55(5)° $\sum_{(Cu3)}$ = 12.56(5)°	24b
SiF_6^{-2}	8/3	Cu···Cu = 3.855, 3.886, 3.904 Cu1−N11 = 2.065 Cu2−N12 = 2.069 Cu1−N21 = 2.329 Cu2−N22 = 1.985 Cu1−N31 = 2.006 Cu2−N41 = 1.992 Cu2−N51 = 2.317 Cu3−N42 = 2.353 Cu3−N52 = 2.048 Cu4−N72 = 2.314 Cu3−N62 = 2.039 Cu4−N82 = 2.082 Cu3−N71 = 2.030 Cu4−N92 = 2.019 Cu3−N82 = 2.031 Cu3−N91 = 2.039	abc abc	triclinic/$P\bar{1}$	$\sum_{(Cu1)}$ = 10.96(5)° $\sum_{(Cu2)}$ = 15.87(5)° $\sum_{(Cu3)}$ = 25.47(5)° $\sum_{(Cu4)}$ = 13.44(5)°	24b
ZrF_6^{-2}	1	Cu···Cu = 3.8850(3) Cu1−N1 = 2.299(3) Cu2−N12 = 2.385(3) Cu1−N21 = 2.080(3) Cu2−N2 = 2.023(3) Cu1−N11 = 2.014(3) Cu2−N22 = 2.029(3)	ab ab ab	monoclinic/$P2_1/n$	$\sum_{(Cu1)}$ = 12.76(5)° $\sum_{(Cu2)}$ = 19.44(5)°	20
NO_3^-	1	Cu···Cu = 3.903(1)	ab ab ab	monoclinic/$C2/c$	$\sum_{(Cu1)}$ = 13.00(5)°	this work

is 13.223(4) Å. All 1,2,4-triazole rings are planar; the deviation from the least-squares plane through the ring atoms is smaller than 0.18 Å. The crystal packing is formed by an infinite octahedral array of $[Cu(NH_2trz)_3]^{2+}$ linear chains running along the *c* axis, with two NO_3^- counteranions and a non-coordinated water molecule in the vacancies (Figure 5a). Many intra- and inter-chain H-bonding interactions involving the nitrate with the non-coordinated water molecule and with the amino group of the triazole ring, are found (Figure 5).

Intra-chain interactions are clearly identified between triazoles belonging to the same chain and the nitrate anion. Indeed, two amino groups of a triazole, of the A and B planes, are connected through H-bonding to two different oxygen atoms of the same nitrate group: N5−H5A···O1 at 3.126 Å and N1−H1A···O3 at 3.224 Å (Figure 5b). An additional H-bond is found between the amino group of the A plane and the O2 atom of the nitrate at 3.229 Å (N5−H5A···O2). A bifurcated H-bonding type is also found between O1 atom of nitrate and the −C−H of triazole rings in two different planes, C2−H2···O1 and C3−H3···O1 at 3.087 Å and 3.048 Å, respectively (Figure 5b).

In the B plane, the second NO_3^- group makes short intramolecular interactions between (a) the -NH_2 groups of two adjacent triazole rings, N1−H1A···O1 at 3.151 Å and N1−H1A···O2 at 3.159 Å; (b) the −C−H of two different triazole rings at 3.125 Å (C1−H1···O3) and at 3.129 Å C2−H2···O3 (Figure 5c).

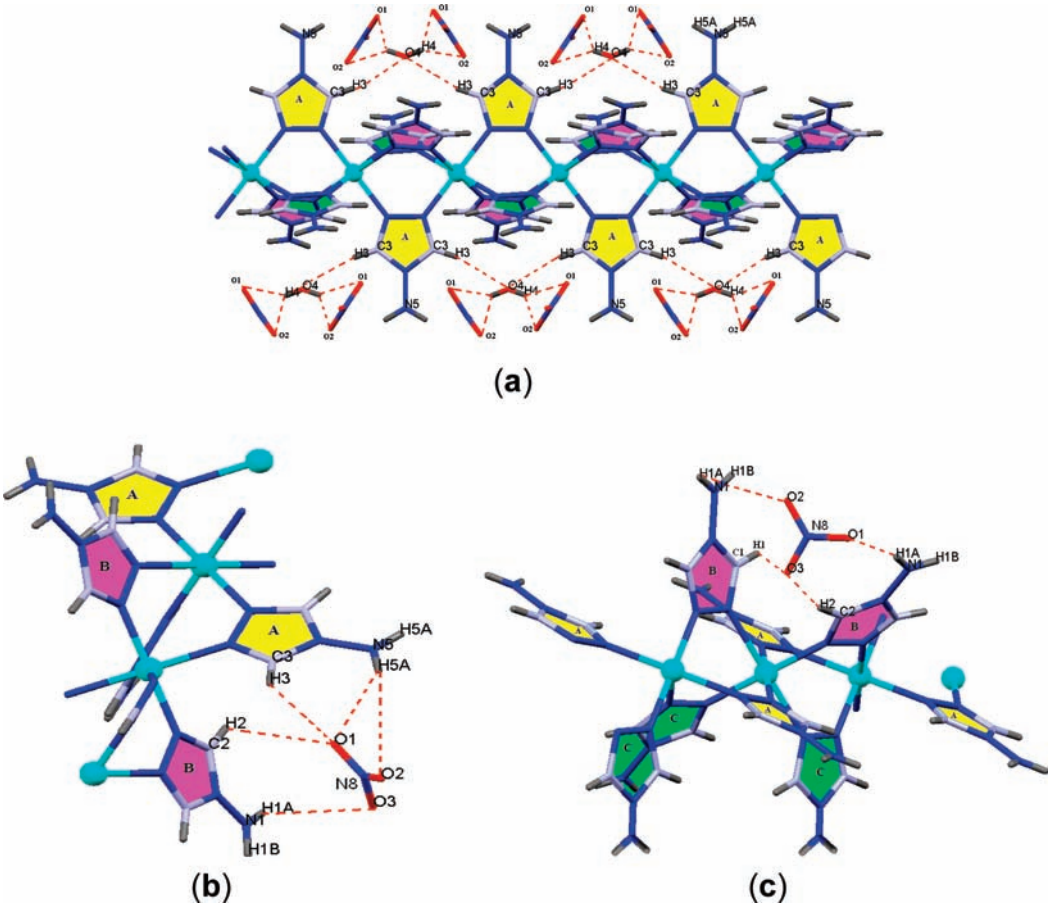

Figure 5. Intra-chain H-bonds interactions involving H_2O or nitrate for **2**: (a) the water molecule is connected to neighboring triazole (in yellow) by C−H···O interactions. (b) A nitrate is found to link the −C−H and the amino group of two triazole ring belonging to different planes (A in yellow and B pink). (c) A nitrate is connected to two amino groups and C−H of two triazole rings located in the B plane.

The water molecule also connects two octahedra within a chain by C−H···O interactions through the triazole rings of the A plane at 3.215 Å (C3−H3···O4). The same water molecule is connected through H-bonding to oxygen atoms of nitrate groups at 3.339 Å (O4−H4···O1) and at 2.931 Å (O4−H4···O2) (Figure 5a). This water molecule is located between the chains and forms two bifurcated H-bonds with two nitrate which are related to different chains thanks to electrostatic interactions thus establishing indirect inter-chain interactions (Figure 6a). In addition, the nitrate anions strengthen inter-chain interactions; a trifurcated hydrogen interaction is found for O1, with amino groups belonging to two different chains, N5−H5A···O1 = 3.126 Å, N1−H1A···O1 = 3.151 Å, and with a −CH group of a chain (C2−H2···O1 = 3.087 Å). O2 is also connected to an amino group (N5−H5A···O2 = 3.229 Å) (Figure 6b) and the third oxygen of the nitrate (O3) is connected to a triazole ring (C2−H2···O3 = 3.129 Å).

Nitrate groups are thus implied in different intermolecular interactions (bi- and trifurcated)[29] and set up a dense hydrogen bonding network.

Intramolecular interactions involving a non-coordinated molecule were also identified for related Cu^{II} 4R-1, 2,4-triazole chains.[20b,24b−d] In the case of $[Cu(hyetrz)_3](ClO_4)_2\cdot 3H_2O$ (hyetrz = 4-(2′-hydroxyethyl)-1,2,4-triazole),[3a] a hydrogen bond between hydroxyl groups from the ligands, originating from neighboring triple μ-triazole links is identified as an intra-chain H-bonding lock. In $[Cu(hyetrz)_3](CF_3SO_3)_2\cdot H_2O$,[3b] and in $[Cu(NH_2trz)_3](BF_4)_2\cdot H_2O$,[24b] a weak double hydrogen bonding −C−H···X···H−C− (X = $CF_3SO_3^-$ or BF_4^-) that connect the anions to the chains is found. In $[Cu(NH_2trz)_3]ZrF_6\cdot H_2O$ no hydrogen bonds between the fluorine atom of ZrF_6^{2-} and the −C−H of triazole ring is identified,[20b] but a pseudo three-dimensional (3D) hydrogen bonding network is formed by H-bonding between fluorine atom and the -NH_2 group of the triazole and with the oxygen atom of water molecule. In **2**, the situation is unique because all types of interactions could be identified. The 'tripod' character of nitrate groups allows linking the NH_2trz rings by their −C−H and amino groups, which does rigidify the H-bonding network. The H-bonding network is reinforced by four different hydrogen bonds between water molecule and two different nitrate groups that belong to two different chains, −N−O···H(H_2O)···O−N− by double hydrogen bonding −C−H···X···H−C−. However, the hydrogen bonding network can be overall considered of moderate strength because hydrogen bonds range from 2.931 to 3.339 Å with bond angles varying from 84° to 165°, which deviates from linearity.

(29) Taylor, R.; Kennard, O.; Versichel, W. *J. Am. Chem. Soc.* **1984**, *106*, 244.

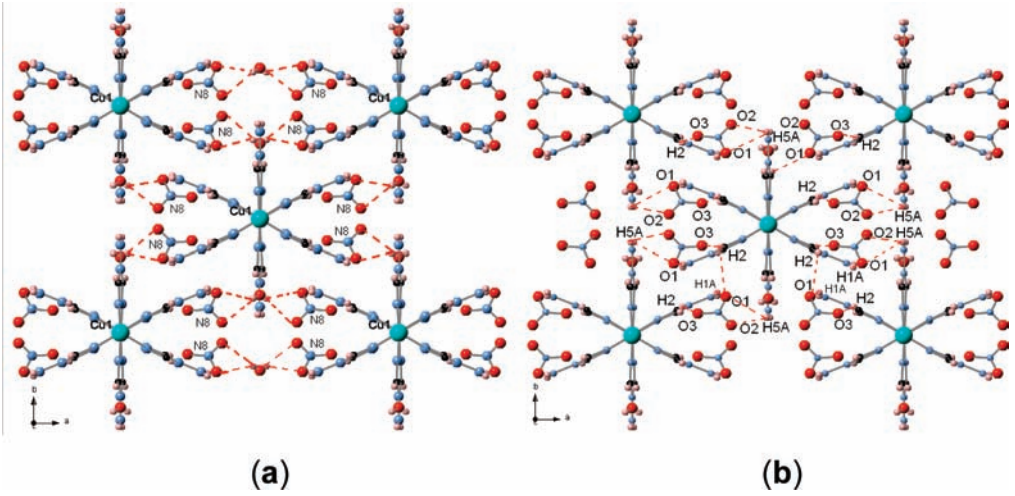

Figure 6. Projection of the crystal structure of **2** on the (*ab*) plane showing intermolecular hydrogen-bonded chains involving (a) both nitrate and water molecule, and (b) nitrate and triazole rings.

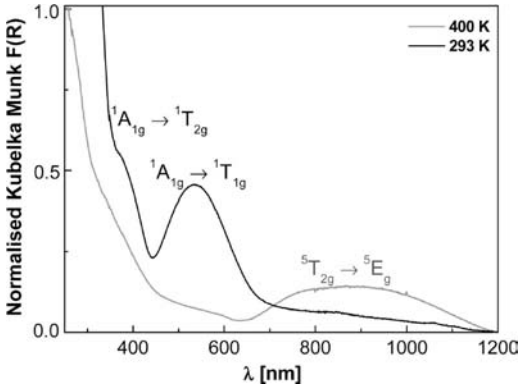

Figure 7. Kubelka−Munk function $F(R)$ of **1** showing the d−d transitions at 293 K and at 400 K.

2.3. Thermally Induced ST in 1. 2.3.1. UV−vis Diffuse Reflectance Spectroscopy. Compound **1** presents a reversible thermochromism from pink to white on warming above room temperature (Figure 7). These colors depend on the spin state of the Fe^{II} centers. The pink color, at 293 K, is due to the $^1A_{1g} \rightarrow {}^1T_{1g}$ d-d transition of LS Fe^{II} sites observed at ~18700 cm^{-1}. A second band identified around 26700 cm^{-1} is attributed to $^1A_{1g} \rightarrow {}^1T_{2g}$ d-d transition. The white color, at 400 K, results from the location of the d-d transition, $^5T_{2g} \rightarrow {}^5E_g$, for the HS sites in the near-infrared region (~12300 cm^{-1}). The ligand field strength for the HS and LS states have been evaluated thanks to eqs 1 and 2.[30]

$$10D_q^{HS} = E(^5E) - E(^5T_2) \quad (1)$$

$$10D_q^{LS} = E(^1T) - E(^1A_1) + \frac{E(^1T_2) - E(^1T_1)}{4} \quad (2)$$

The following values were obtained: $10D_q^{HS} \sim 12300\ cm^{-1}$ and $10D_q^{LS} \sim 25375\ cm^{-1}$. These are typical of Fe^{II} complexes presenting a thermally induced SCO behavior.[30]

2.3.2. ^{57}Fe Mössbauer Spectroscopy. An inspection of the SCO properties for **1** using ^{57}Fe Mössbauer spectroscopy was undertaken over the temperature range 293−380 K (Figure 8a, b). Mössbauer parameters are listed in Table 4, and representative spectra are shown in Figure 8b. The spectrum at 293 K shows one quadrupole doublet attributed to LS Fe^{II} ions ($\delta^{LS} = 0.44$ (1) mm·s^{-1} and $\Delta E_Q^{LS} = 0.19(1)$ mm·s^{-1}) in good agreement with literature data that were only reported at room temperature.[18,19] The detection of a quadrupole splitting stems from a lattice contribution to the electric field gradient which points out to a distortion of the LS octahedra within the chain.[20] The compound remains in the LS state on warming up to 330 K, after which a second quadrupole doublet attributed to HS Fe^{II} ions grows in intensity (e.g., at 342 K, $\delta^{HS} = 0.98(3)$ mm·s^{-1} and $\Delta E_Q^{HS} = 2.59(1)$ mm·s^{-1}). This larger quadrupole splitting is due to the rising of the valence contribution of HS Fe^{II} ions. The relative area fraction of the HS doublet slowly increases to ~38.5% at 346 K and then more abruptly at 351 K where the spectrum consists of a dominant HS doublet, 74% ($\delta^{HS} = 0.99$ (1) mm·s^{-1} and $\Delta E_Q^{HS} = 2.57(2)$ mm·s^{-1}). The slight asymmetry of the lines observed in the HS state is attributed to a texture effect. After this temperature the relative area of HS Fe^{II} ions increases again slowly to reach 92% at 380 K, with $\delta^{HS} = 0.97(1)$ mm·s^{-1} and $\Delta E_Q^{HS} = 2.49(1)$ mm·s^{-1}, indicating an incomplete ST at this temperature. Upon cooling to room temperature, the reverse situation is observed. The spectra shown on cooling and warming modes at 330 K clearly evidence a hysteretic effect (Figure 8b). Indeed, the ST curve deduced by plotting the variation of the temperature dependence of the HS molar fraction, γ_{HS}, shows a hysteresis loop, with $T_c^{\uparrow} = 347(1)$ K and $T_c^{\downarrow} = 317(1)$ K (Figure 8a). These values are in good agreement with the ones obtained by magnetic susceptibility measurements

(30) (a) Gütlich, P.; Jung, J.; Goodwin, H. A. Spin Transitions in Iron(II) Complexes. An Introduction In *Molecular Magnetism: From Molecular Assemblies to the Devices*; Kluwer Academic: Dordrecht , The Netherlands, 1996; p 327. (b) Gütlich, P.; Hauser, A.; Spiering, H. *Angew. Chem., Int. Ed. Engl.* **1994**, *33*, 2024. (c) Gütlich, P.; Hauser, A.; Spiering, H. In *Inorganic Electronic Structure and Spectroscopy*; A. B. Lever, P., Solomon, E. I., Eds.; John Wiley & Sons: New York, 1999; Vol. *II*, p 575. (d) Gütlich, P.; Garcia, Y.; Goodwin, H. A. *Chem. Soc. Rev.* **2000**, *29*, 419. (e) Gütlich, P.; Garcia, Y.; Spiering, H. *Magnetism: From Molecules to Materials IV*; Wiley-VCH: New York, 2003; p 271. (f) Gütlich, P.; Goodwin, H. A. Spin Crossover in Transition Metal Compounds. In *Topics in Current Chemistry*; Springer: Berlin-Heidelberg, 2004; pp 233−235.

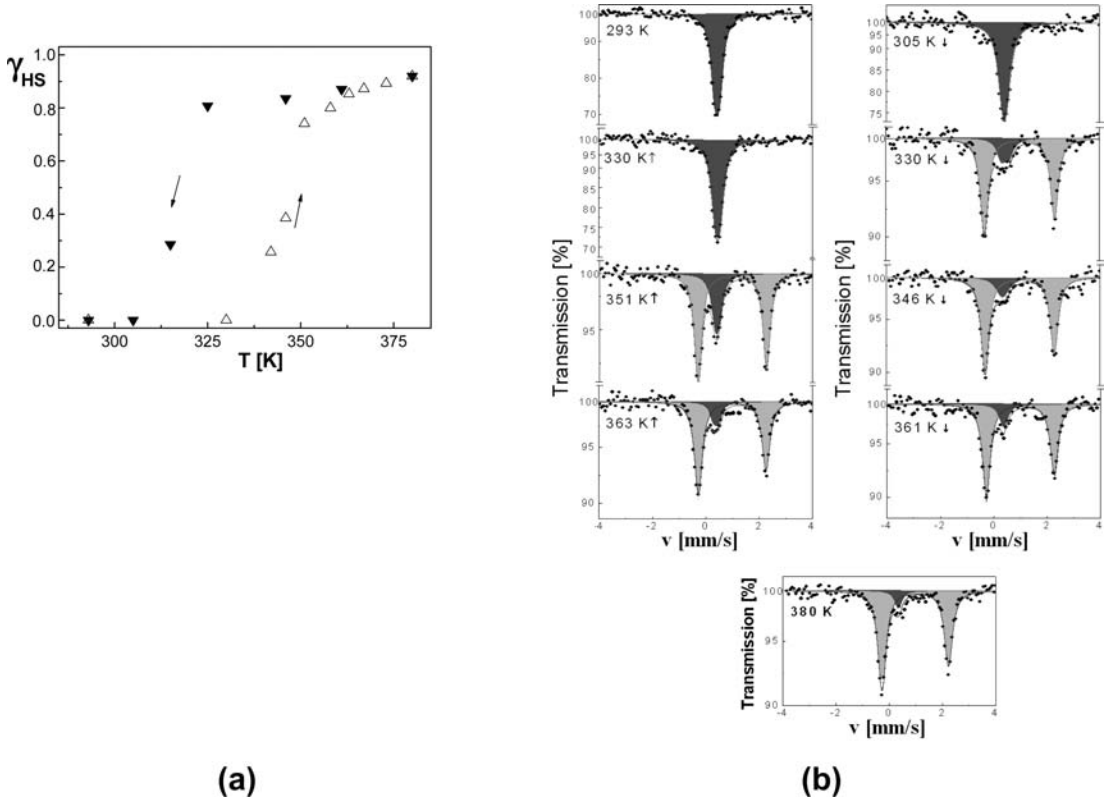

Figure 8. (a) γ_{HS} vs T curves on cooling (▼) and on warming (△) modes for **1**. (b) Selected ^{57}Fe Mössbauer spectra of **1** on warming and on cooling mode. Gray and dark gray correspond to the HS and LS doublets, respectively.

Table 4. Overview of the ^{57}Fe Mössbauer Parameters for **1** on Warming and on Cooling Mode, over the Temperature Range 293−380 K

T [K]	δ^a [mm/s]	$\Delta E_Q{}^b$ [mm/s]	$\Gamma/2$ ^{c} [mm/s]	relative area [%]	sites
293(1)	0.44(1)	0.19(1)	0.16(2)	100	LS
330(1) $^{\uparrow}$	0.45(1)	0.18(1)	0.19(1)	100	LS
342(1) $^{\uparrow}$	0.98(3)	2.59(1)	0.17(1)	25.7	HS
	0.41(1)	0.16(1)	0.16(1)	74.3	LS
346(1) $^{\uparrow}$	1.03(3)	2.59(1)	0.18(2)	38.5	HS
	0.42(1)	0.16(3)	0.15(1)	61.5	LS
351(1) $^{\uparrow}$	0.99(1)	2.57(2)	0.16(2)	74.0	HS
	0.41(1)	0.13(2)	0.16(1)	26.0	LS
358(1) $^{\uparrow}$	0.99(1)	2.55(1)	0.17(1)	80.0	HS
	0.35(1)	0.19(1)	0.2^d	20.0	LS
363(1) $^{\uparrow}$	0.99(1)	2.54(1)	0.17(1)	85.3	HS
	0.38(2)	0.19(1)	0.15^d	14.7	LS
380(1)	0.97(1)	2.49(1)	0.17(1)	92.0	HS
	0.34(1)		0.15^d	8.0	LS
361(1) $^{\downarrow}$	0.99(1)	2.54(2)	0.17(1)	87.0	HS
	0.37(1)	0.0(1)	0.18(1)	13.0	LS
346(1) $^{\downarrow}$	0.99(1)	2.59(2)	0.17(1)	83.6	HS
	0.35(1)	0.16^d	0.27(1)	16.4	LS
330(1) $^{\downarrow}$	1.00(1)	2.63(2)	0.17(2)	80.8	HS
	0.45(1)	0.29(1)	0.20(1)	19.2	LS
315(1) $^{\downarrow}$	1.01(1)	2.69(1)	0.16(1)	28.6	HS
	0.42(1)	0.17(1)	0.16(1)	71.4	LS
305(1) $^{\downarrow}$	0.44(1)	0.17(1)	0.20(1)	100	LS
293(1) $^{\downarrow}$	0.44(1)	0.19(1)	0.17(2)	100	LS

$^a\delta$ = isomer shift relative to α-iron. $^b\Delta E_Q$ = quadrupole splitting. $^c\Gamma/2$ = half width at half-maximum. ^{d}Fixed parameters. $^{\downarrow}$Cooling. $^{\uparrow}$Warming.

$T_c^{\uparrow} = 348$ K and $T_c^{\downarrow} = 313$ K,[18] μSR spectroscopy $T_c^{\uparrow} = 346$ K and $T_c^{\downarrow} = 312$ K,[19] DSC and XRPD at variable temperature (vide infra).

2.3.3. X-ray Powder Thermo-Diffractometry. The rather resolved X-ray powder diffraction pattern of **1** at 293 K (Figure 3) prompted us to investigate its thermo-diffractometry on warming to track the ST and an eventual crystallographic phase transition that could be at the origin of the observed hysteresis loop. X-ray diffraction patterns of **1** were thus recorded on cooling and warming over the same temperature range investigated by Mössbauer spectroscopy (298−380 K), where the ST reversibly proceeds. The heating/cooling rate was fixed at 10 K/min between each temperature step. Figure 9a shows typical diffraction patterns which are found to be similar on cooling and on warming mode and suggest that there is no crystallographic phase transition over the temperature variation. The intensity of a peak at $2\theta = 24.6°$, corresponding to the HS state, was selected as a marker to follow the ST and the hysteresis loop of **1**, which is included in Figure 9b. On warming, the intensity of the peak at 24.3°, corresponding to the LS state, decreases in favor of the HS peak (Figure 9b). The peaks recorded for intermediate temperatures consist of the sum of these two contributions. The transition temperatures derived from the evolution of $I^{HS}(T)$ are $T_c^{\uparrow} = 347$ K and $T_c^{\downarrow} = 314$ K. These values agree very well with those obtained, for example, by Mössbauer spectroscopy and by μSR.[19] Indexation of the 10 most intense peaks of the diffractogram of **1** (Figure 9), at 293 K (LS) and 380 K (HS), provided preliminary unit cell parameters: at 293 K, $a = 11.83(2)$ Å, $b = 9.72(1)$ Å, $c = 6.361(9)$ Å, $V = 728.585$ Å^3, and at 380 K, $a = 14.37(2)$ Å, $b = 9.61(4)$ Å, $c = 6.76(4)$ Å, $V = 941.501$ Å^3. An elongation of the a axis along with a large volume change of 212.92 Å^3 and a preservation of an orthorhombic primitive lattice, are observed for **1**. A full Rietveld analysis was not possible

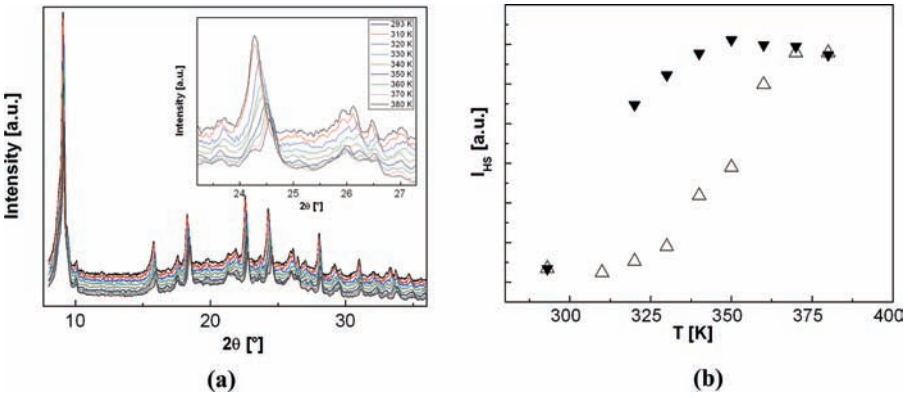

Figure 9. (a) X-ray powder diffraction of **1**, recorded on warming, between 293 and 380 K. The inset shows a zoom of the X-ray powder diffraction recorded on warming. (b) The temperature dependence of the relative intensity of the HS phase I^{HS} peak at $2\theta = 24.6°$, the data were recorded on cooling (▼) and warming (Δ) modes.

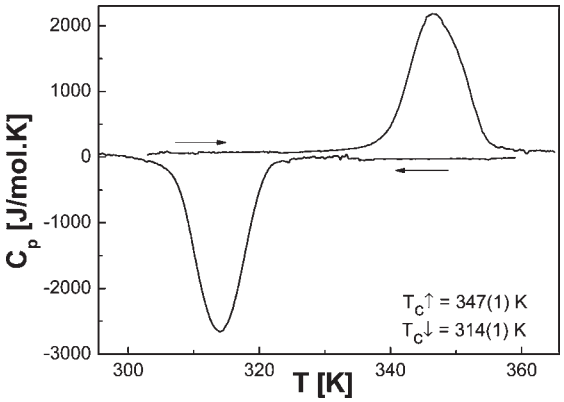

Figure 10. DSC profile of **1** in the 293−400 K temperature range in the cooling (←) and warming (→) modes.

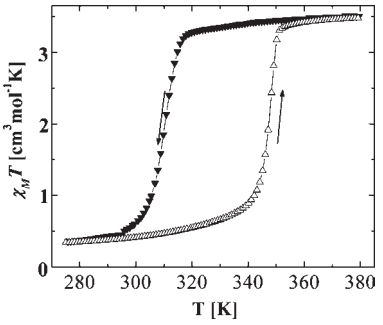

Figure 11. $\chi_M T$ versus T plot for **1** over the temperature range 274−380 K.

because of the presence of broad peaks and a low signal/noise ratio. Assuming 2 molecules in the asymmetric unit, as in the analogous compound **2**, the volume change per unit chain would be 106 Å^3. This value is a 4-fold increased compared to ΔV_{HL} which is the volume difference between HS and LS states for mononuclear complexes (∼ 25 Å^3).[28] For **1**, one should consider the combined effect of thermal dilatation, spin state change of the FeN_6 core, along with variation of interactions between the counteranions and the ligands of the 1D dimensional chains.

2.3.4. DSC. Differential scanning measurements of **1** were carried out at a scan rate of 10 K/min over the temperature range 293−400 K on warming and cooling modes. An endothermic peak is observed on warming at $T_{max}^{\uparrow}$ = 347 K and an exothermic peak is recorded at $T_{max}^{\downarrow}$ = 314 K, on cooling, thus revealing a hysteresis loop of width 33 K (Figure 10). This behavior is characteristic of a first-order phase transition and can be related to the ST detected by magnetic measurements,[18] XRPD, and Mössbauer spectroscopy studies. The enthalpy and entropy variation have been evaluated as ΔH = 23(1) kJ mol^{-1} and ΔS = 69.6(1) J mol^{-1} K^{-1}. The enthalpy variation agrees well with the one obtained by isobaric heat capacity measurements ΔH = 22.8(4) kJ mol^{-1}.[31] The vibrational contribution to the entropy variation is evaluated as ΔS_{vib} = 56.2 J mol^{-1} K^{-1}, the electronic contribution being equal to R ln5 = 13.4 J mol^{-1} K^{-1} for Fe^{II} SCO compounds.[30] These entropy values are somewhat larger than usually observed for Fe^{II} mononuclear SCO compounds,[32] but conforms well with the strong cooperative nature of the ST for this 1D coordination polymer.[9,15]

2.3.5. Magnetic Susceptibility Measurements. SQUID Investigation. The magnetic data were collected over the temperature range 274−380 K on warming and cooling modes under an applied field of 1000 Oe. The temperature dependence of the molar magnetic susceptibility is displayed in Figure 11 in the form of a $\chi_M T$ versus T plot, χ_M being the molar magnetic susceptibility per Fe^{II} ion corrected for diamagnetic contributions. At 274 K, $\chi_M T$ is equal to 0.34 cm^3 mol^{-1} K, which indicates Fe^{II} ions in the LS state with few paramagnetic ions that were also identified at room temperature in a previous ^{57}Fe Mössbauer spectrum.[19] Such HS ions were not detected in our Mössbauer investigation (Figure 8b) presumably because of the less resolution of our spectrum (compared with the one from the reference study[19]). As T is increased, $\chi_M T$ progressively increases reaching about 0.8 cm^3 mol^{-1} K around 338 K, after which $\chi_M T$ increases sharply at 352 K. Above this temperature, $\chi_M T$ increases very slowly and shows a plateau of 3.47 cm^3 mol^{-1} K at 380 K, which

(31) Bessergenev, V. G.; Berezovskii, G. A.; Lavrenova, L. G.; Larionov, S. V. *Zh. Fiz. Khim.* **1997**, *71*, 809.

(32) König, E. *Struct. Bonding* (*Berlin*) **1991**, *76*, 51.

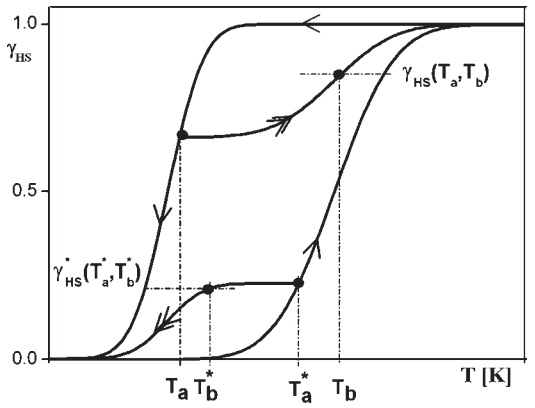

Figure 12. Thermal FORC in warming/cooling modes.[34].

indicates HS Fe^{II} ions. In the cooling mode, as the temperature is decreased, $\chi_M T$ follows the same pathway as that observed when warming except in the range 350−319 K, which indicates a hysteresis loop ~37 K wide centered at 328 K. The transition temperatures at which 50% of active LS and HS molecules are present in the warming and cooling modes are $T_c^{\uparrow} = 347(1)$ K and $T_c^{\downarrow} = 310(1)$ K. The hysteresis loop is retained over successive cooling and heating thermal cycles, which confirm the ST reversibility of **1**.

FORC Diagram Investigation. The recording of magnetic measurements in DC mode reported above only provides a primary analysis of the hysteresis loop of **1**. We have extended this study by recording First-Order Reversal Curves (FORCs) to determine the distribution of switching temperatures and interactions fields for all of the 'particles' that contribute to the hysteresis loop.[33] FORCs actually represents a specific class of minor hysteresis loops, for which the sweeping process of the input parameter, here temperature, is reversed only once.[34] The measurement of a FORC begins with the saturation of the sample in the HS (or LS) state, where $\gamma_{HS} = 1$ (or $\gamma_{HS} = 0$). The temperature is then ramped down (or up) to a reversal temperature called T_a (or T_a*). The FORC consists of a measurement of γ_{HS} as the temperature is then increased from T_a (or T_a*) back up (or down) to saturation. The HS fraction at T_b (or T_b*) on the FORC with reversal point T_a is denoted by $\gamma_{HS}(T_a,T_b)$ (see Figure 12). Two sets of FORCs data can thus be recorded, but here we have restricted ourselves to one mode (vide infra).

The temperature step is chosen with T_a and T_b being regularly spaced, which means that $\gamma_{HS}(T_a,T_b)$ can be plotted on a regular grid. We also define the equilibrium temperature in the frame of an Ising like model as

$$T_{1/2} = \frac{\Delta}{k_B \ln g} \tag{3}$$

where $g = g_{HS}/g_{LS}$ is the ratio of the degeneracy of states, which results from the change in entropy for a total spin conversion ($\Delta S = R \ln g$), R is the gas constant).[35]

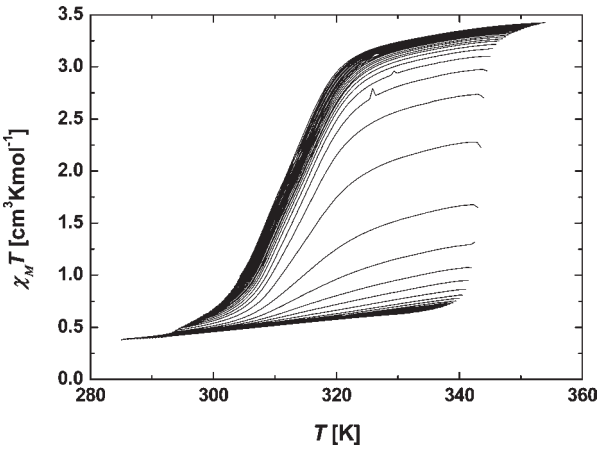

Figure 13. FORCs of the thermal hysteresis loop of **1** recorded in the cooling mode, with T_a, T_b increments of 0.5 K.

The FORC distribution $\rho(T_a,T_b)$ is defined as the mixed second derivative:

$$\rho(T_a, T_b) = -\frac{\partial^2 \gamma_{HS}(T_a, T_b)}{\partial T_a \partial T_b} \tag{4}$$

and plotted with rotated axes from switching temperatures (T_a,T_b) to a "bias" (b)−"coercivity" (c) diagram following eqs 5 and 6, respectively.

The b and c parameters are defined as follows:

$$b = \frac{T_a + T_b}{2} \tag{5}$$

$$c = \frac{T_a - T_b}{2} \tag{6}$$

The "bias" parameter, which is related to the equilibrium temperature $T_{1/2}$, roughly corresponds to the energy gap Δ between HS and LS states. The "coercivity", which is related to the width of the thermal hysteresis loop, reflects the strength of intra-domain interactions, which is characterized by the J parameter.[35,36] J is an interaction parameter derived from a two-level Ising like description of interacting SCO units.

Figure 13 shows the experimental FORCs for **1** obtained on a SQUID magnetometer. The sample was slowly warmed up to a reversal temperature located on the upper branch of the hysteresis loop, and the sample was subsequently cooled. The temperature step was fixed at 0.5 K for both T_a and T_b, with a sweeping rate of 0.8 K/min. It was essential to use such a small temperature step to obtain the best accurate data.[35] Kinetic effects were also avoided by working in cooling mode only. Indeed, preliminary measurements attempted in the warming mode revealed that it was not possible to fix the reversal temperature on the lower branch of the hysteresis loop because of the thermal inertia of the SQUID magnetometer.

(33) Pike, C. R.; Roberts, A. P.; Verosub, K. L. *J. Appl. Phys.* **1999**, *85*, 6660.
(34) Tanasa, R.; Enachescu, C.; Stancu, A.; Varret, F.; Linares, J.; Codjovi, E. *Polyhedron* **2007**, *26*, 1820.
(35) Enachescu, C.; Tanasa, R.; Stancu, A.; Codjovi, E.; Linares, J.; Varret, F. *Phys. B* **2004**, *343*, 15.
(36) Tanasa, R.; Enachescu, C.; Stancu, A.; Codjovi, E.; Linares, J.; Varret, F.; Haasnoot, J. G. *Phys. Rev. B* **2005**, *71*, 014431.

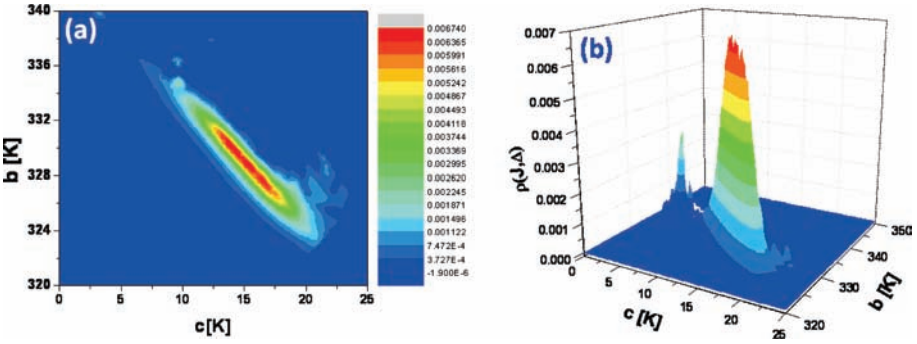

Figure 14. Experimental FORC diagram derived from Figure 13, in coercivity-bias coordinates: (a) 2D contour plot representation and (b) 3D representation.

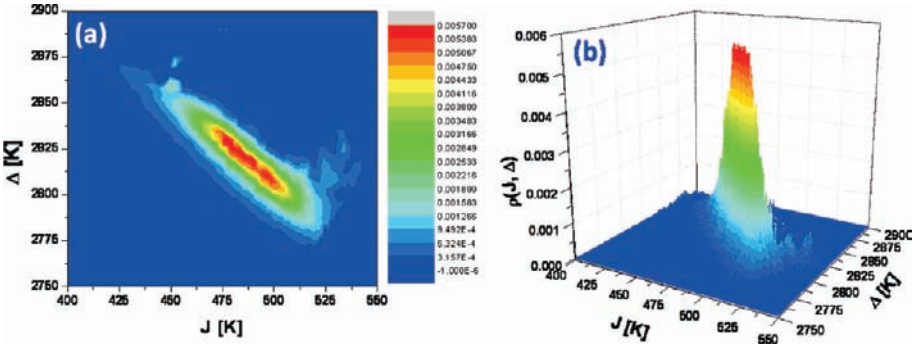

Figure 15. Experimental joint FORC diagram in J-Δ coordinates: (a) 2D contour plot representation and (b) 3D representation.

Table 5. Statistical Analysis of the FORC Distributions from Figure 14

$\overline{b}^a$ [K]	$\sigma(b)$ [K]	$\overline{c}^a$ [K]	$\sigma(c)$ [K]	$r_{c,b}$	$\overline{\Delta}^a$ [K]	$\sigma(\Delta)$ [K]	$\mathcal{J}^a$ [K]	$\sigma(J)$ [K]	$r_{J,\Delta}$
329.4	3.7	14.7	4.4	−0.67	2813	20	496.4	17.8	−0.75

[a] $\overline{b}$, $\overline{c}$, $\overline{\Delta}$, $\mathcal{J}$ represent the mean values of the parameters b, c, Δ, and J, respectively.

As it has been shown in ref 36 by using the Jacobian transformation, a correspondence can be performed between FORC distributions in c-b and J-Δ coordinates. The FORC diagram is actually a 3D image represented by the 2D contour plot of the FORC distribution. Colors provide information about the probability that a single domain could be characterized by a given value c-b or J-Δ (Figure 14, 15). The probability is very low in the blue region and becomes very high in the red region. In the present case, an interaction parameter J = 496 K and an energy gap Δ = 2813 K were obtained (Table 5). It is much higher than the one found for the two-dimensional (2D) ST compound $[Fe(btr)_2(NCS)_2]\cdot H_2O$ (J = 235 K)[36] which presents a hysteresis width of 25 K,[37] free of any structural phase transition,[5,38] compared to 33 K for **1**.

We have also performed a statistical analysis after the procedure described in ref 36 that allowed us to derive the average values of bias ($\overline{b}$), coercivity ($\overline{c}$), the standard deviations, σ(b) and σ(c), and the dimensionless correlation parameter $r_{c,b}$ (Table 5). It represents the degree of correlation between the joint distributions following eq 7.

$$r_{c,b} = \mathrm{cov}(b,c)/\sigma(b)\sigma(c) \qquad (7)$$

A negative correlation is found with $r_{c,b}$ = −0.67 and $r_{\Delta,J}$ = −0.75, which is altered on the FORC diagram by a rotation of the distribution counter-clockwise. A similar effect has been observed in diluted $[Fe_xM_{1-x}(btr)_2(NCS)_2]\cdot H_2O$ 2D SCO materials (M^{II} = Zn, Co, Ni), where the correlation parameter increases with increasing dilution.[35,39] Such correlation may be ascribable to the counteranion effect on the chains which is acting as a negative pressure on these.[20] A detailed study of this effect could be part of a future work where the size of the counteranion will be modified to track a correlation between the counteranion size and the cooperativity of the system.

3. Discussion

The exclusive ST properties of $[Fe(NH_2trz)_3](NO_3)_2$ (**1**) being associated to an unusually large hysteresis loop feeds the debate about the origin of cooperative effects for 1D 1,2,4-triazole Fe^{II} chain compounds.[5,10] A crystallographic

(37) Vreugdenhil, W.; Van Diemen, J. H.; De Graaff, R. A. G.; Haasnoot, J. G.; Reedijk, J.; Van der Kraan, A. M.; Kahn, O.; Zarembowitch, J. *Polyhedron* **1990**, *9*, 2971.

(38) (a) Garcia, Y.; Gieck, C.; Stauf, S.; Tremel, W.; Gütlich P. 4th TMR TOSS-Meeting, Bordeaux, France, **2001**. (b) Pillet, S.; Hubsch, J.; Lecomte, C. *Eur. Phys. J. B* **2004**, *38*, 541.

(39) Rotaru, A.; Dîrtu, M. M.; Enachescu, C.; Tanasa, R.; Linares, J.; Stancu, A.; Garcia, Y. *Polyhedron* **2009**, *28*, 2531.

phase transition that would occur concomitantly with the ST[40] could explain the increase of hysteresis width for **1** compared to other NH_2trz chains that also present an hysteretic ST but of lower width (Figure 1). This situation has already been encountered for instance for Fe^{II} mononuclear complexes $[Fe(1\text{-}n\text{-propyl-tetrazole})_6](BF_4)_2$,[41] and $[Fe(PM\text{-}AzA)_2(NCS)_2]$ (PM = *N*-2′-pyridylmethylene, AzA = 4-(phenylazo)aniline),[42] that both display a ST on cooling below room temperature. XRPD patterns recorded on warming at variable temperatures for **1** have, however, revealed the absence of a crystallographic phase transition (Figure 9), a result which was confirmed by DSC that did not reveal an unusually large entropy value.[32] The hysteresis width developed by **1** can thus fully be ascribed to solid state cooperative effects that have been investigated in this work.

The transition temperatures and the hysteresis width are usually employed to characterize hysteretic SCO curves and to establish comparisons between SCO systems.[30] However, because of the various combinations of ligands, anions, grain size, internal stress, and elastic interactions among active SCO sites, different systems can be characterized by the same transition temperatures and even by the same external thermal envelope of the hysteresis loop, whereas a completely different behavior occurs within their hysteresis loop, particularly regarding domain distributions.[43] In an attempt to remove some of the ambiguities inherent to conventional hysteresis measurements, Pike et al. developed a novel characterization tool based on First-Order Reversal Curve (FORC) measurements.[33] It was also successfully used for the characterization of other systems presenting hysteretic behavior such as ferroelectric materials,[44] nanowires,[45] multilayers,[46] spin glasses,[47] and ST materials presenting pressure, thermal, and light induced thermal hysteresis.[48−50] On the basis of the thermodynamic characterization of **1** derived by DSC, the extent of cooperative effects effective in **1** was probed, for the first time in a 1D SCO system, through a FORC investigation. The mean value of the interaction parameter derived from this FORC analysis was evaluated as $J = 496$ K. This value is relatively high and suggests that intra-chain interactions between the spin active molecules play an important role on the cooperativity of this system (section 2.3.5). Furthermore, the FORC diagram reveals a strong correlation between distributions in *c*-*b* and J-Δ coordinates which has been attributed to an internal pressure effect induced by the nitrate anion on the chain.

Since Fe^{II}−1,2,4-triazole systems hardly crystallize, because of insolubility of the coordination polymers and potential Fe(II) oxidation, it was necessary to obtain single crystals of an analogous material containing a nitrate anion so as to gain further insights to the ST phenomenon of **1**. Hydrothermal pretreatement as a method of recrystallization of 1D chains was proposed and provided single crystals of **2** suitable for a X-ray analysis. The first crystal structure of a 1D chain triazole derivative with a nitrate anion was thus obtained. It also represents one of the rare example of crystallized 1D chain complexes with triple *N*1,*N*2-1,2,4-triazole bridges.[3,16,20b,24] The crystal structure of **2** is stabilized by a sophisticated and dense hydrogen bonding network, involving the nitrate, the amino group of the triazole ligand and a non-coordinated water molecule (Figure 6b). The anion is bonded to both amino groups of adjacent triazole molecules belonging to two 1D chains setting up inter-chain interactions. Thus, each chain is hydrogen bonded to four others, only by implication of the nitrate group with the ligand ($-NH_2$, $-C-H$) of different neighboring chains. Intra-chain interactions are identified between the nitrate groups and the amino groups of two adjacent (in the same or in different planes) triazole rings. Intra-chain interactions are also found between a non-coordinated water molecule and $-C-H$ of two triazole rings within the chain. The water molecule (Figure 4b) plays a double role because it participates in intermolecular interactions and increase supramolecular contacts between the chains. We thus conclude on the relevance of water molecules in the stabilization of the structure, which relates two different NO_3^- groups, involved also in intra- and inter-chain interactions in different chains. Indeed this stabilization is supported by the systematic single crystals degradation of **2** into a powder observed by taking out the samples from the mother solution at room temperature and ambient pressure.

Intra- and intermolecular interactions are thus assumed to strengthen elastic interactions between switching centers in **1**, thus resulting in a wide hysteresis loop. Such interactions may not only be facilitated by the planar geometry of the nitrate anion but also by its "tripod" character. In particular, the role of the nitrate anion that acts as a fourth supramolecular bridge in addition to the triple 1,2,4-triazole bridge between metallic centers is pointed out (Figure 5b). This extra-bridge is believed to strengthen elastic interactions within the chain of **1** compared to classic chains that show hysteresis of lower width (Figure 1). These findings are consistent with the literature. Indeed, it was observed for **1** by μSR spectroscopy[19] that the amino group of the 1,2,4-triazole cannot freely rotate as a consequence of its likely hydrogen bonding to a nitrate anion that would support intra-and inter-chain interactions claimed for **1**. It is worthwhile to note that the role of hydrogen bonds to promote wide hysteresis loop has also recently been recognized in SCO research for an iron(II) mononuclear material presenting a 70 K wide hysteresis loop around room temperature.[51]

(40) Kusz, J.; Gütlich, P.; Spiering, H. *Top. Curr. Chem.* **2004**, *234*, 129.
(41) Jeftić, J. *High Press. Res. Int. J.* **2009**, *2*, 369.
(42) Létard, J.-F.; Guionneau, P.; Codjovi, E.; Lavastre, O.; Bravic, G.; Chasseau, D.; Kahn, O. *J. Am. Chem. Soc.* **1997**, *119*, 10861.
(43) (a) Sorai, M.; Seki, S. *J. Phys. Soc. Jpn.* **1972**, *33*, 575. (b) Chong, C.; Berini, B.; Boukheddaden, K.; Codjovi, E.; Linares, J.; Garcia, Y.; Naik, A. D.; Varret, F. *Phys. Status Solidi A* **2010**, *207*, 1227.
(44) (a) Stancu, A.; Ricinschi, D.; Mitoseriu, L.; Postolache, P.; Okuyama, M. *Appl. Phys. Lett.* **2003**, *83*, 3767. (b) Stancu, A.; Mitoseriu, L.; Stoleriu, L.; Piazza, D.; Galassi, C.; Ricinschi, D.; Okuyama, M. *Phys. B* **2006**, *372*, 226.
(45) (a) Beron, F.; Clime, L.; Ciureanu, M.; Menard, D.; Cochrane, R. W.; Yelon, A. *J. App. Phys.* **2007**, *101*, 09J107/1. (b) Lavin, R.; Denardin, J. C.; Escrig, J.; Altbir, D.; Cortes, A.; Gomez, H. *IEEE Trans. Magn.* **2008**, *44*, 2808.
(46) (a) Davies, J. E.; Hellwig, O.; Fullerton, E. E.; Denbeaux, G.; Kortright, J. B.; Liu, K. *Phys. Rev. B* **2004**, *70*, 224434. (b) Yin, J.; Zhang, H.; Hu, F.; Shen, B.; Pan, L. Q. *J. Appl. Phys.* **2009**, *106*, 103901/1.
(47) (a) Katzgraber, H. G.; Pazmand, F.; Pike, C. R.; Liu, K.; Scalettar, R. T.; Verosub, K. L.; Zimanyi, G. T. *Phys. Rev. Lett.* **2002**, *89*, 257202. (b) Katzgraber, H. G.; Herisson, D.; Osth, M.; Nordblad, P.; Ito, A.; Katori, H. A. *Phys. Rev. B* **2007**, *76*, 092408/1.
(48) (a) Enachescu, C.; Tanasa, R.; Stancu, A.; Varret, F.; Linares, J.; Codjovi, E. *Phys. Rev. B* **2005**, *72*, 054413. (b) Enachescu, C.; Tanasa, R.; Stancu, A.; Varret, F.; Linares, J.; Codjovi, E. *Phys. B* **2006**, *372*, 211.
(49) (a) Tanasa, R.; Stancu, A.; Létard, J. -F.; Codjovi, E.; Linares, J.; Varret, F. *Chem. Phys. Lett.* **2007**, *443*, 435. (b) Tanasa, R.; Stancu, A.; Codjovi, E.; Linares, J.; Varret, F.; Létard, J.-F. *J. Appl. Phys.* **2008**, *103*, 07B905.
(50) Tanasa, R.; Linares, J.; Enachescu, C.; Varret, F.; Stancu, A. *Phys. B* **2006**, *372*, 215.
(51) Weber, B.; Bauer, W.; Obel, J. *Angew. Chem., Int. Ed.* **2008**, *47*, 10098.

4. Concluding Remarks

The origin of the wide hysteresis loop occurring above room temperature for $[Fe(NH_2trz)_3](NO_3)_2$ has been discussed in light of a careful examination of the magnetic properties along with DSC, Mössbauer, and structural studies. This study confirms that intramolecular interactions realized by triply 1,2,4-triazole bridges connecting spin changing molecules as well as intermolecular interactions mediated by a tripodal planar anion can promote strong cooperative effects,[5] resulting in the observation of large hysteresis width, free of any structural phase transition. Because the ST of this material is accompanied by an intense color change, such characteristics could be useful for optical data recording or thermal sensing around room temperature.[7] We shall further synthesize and investigate new SCO chains including planar and "poly pods" counteranions to increase the hysteresis width of these materials that can switch their spin states around the room temperature region.

5. Experimental Section

Synthesis. All reagents and solvents were used as received from commercial source: 4-amino-1,2,4-triazole, 99% (ACROS), copper(II) nitrate trihydrate, extra pure (ACROS), iron(II) sulfate heptahydrate (ACROS), barium nitrate (VWR).

$[Fe(NH_2trz)_3](NO_3)_2$ (1). $[Fe(NH_2trz)_3](NO_3)_2$ was synthesized as a pink powder using a procedure described elsewhere.[18] Before all analysis the compound was maintained in vacuum condition to remove the eventual presence of surface water in $[Fe(NH_2trz)_3]NO_3)_2$. Fractional degree of hydration, when exposed to air (0.13 mol H_2O) was confirmed by TGA measurements (Supporting Information, Figure S1).

$[Cu(NH_2trz)_3](NO_3)_2 \cdot H_2O$ (2). An aqueous solution (3 mL) of $Cu(NO_3)_2 \cdot 3H_2O$ (0.0957 g, 0.396 mmol) was added dropwise to a 2 mL aqueous solution of NH_2trz (0.1 g, 1.189 mmol) leading to a blue precipitate. After 30 min of vigorous stirring at room temperature, a blue solid was filtered off in air, washed with distilled water (2 mL), and dried in a desiccator. Yield: 0.1 g, 55%. Anal. for $CuC_6H_{14}N_{14}O_7$ (457.81 g/mol): calcd. C, 15.74; H, 3.08; N, 42.83, Cu, 13.88%. Found: C, 15.88; H, 2.98; N, 42.64, Cu, 13.2%. IR (KBr, cm^{-1}): $\nu(NH_2) \sim 3305$ (w), $\nu_3(N-O) \sim 1384$ (vs), $\nu(N-N) \sim 1218$(w), ν (C−H out of plane) ~ 985(m), $\nu_2(N-O) \sim 827$ (w); ν (C−H ring torsion) ~ 621 (s). Single crystals of $[Cu(NH_2trz)_3](NO_3)_2 \cdot H_2O$ were obtained as follows: 10 mg of **2** was dissolved in distilled water (2 mL) and transferred in a poly(tetrafluoroethylene) container of an acid digestion bomb. The mixture was heated in an oven at 155 °C for 36 h. A small amount of black precipitate formed after reaction was eliminated by filtration at room temperature. The blue filtrate was allowed to stand at room temperature, and blue single crystals in form of needles were obtained by evaporation of the solvent within one week.

Physical Measurements. Elemental analyses were performed at University College London (U.K.). IR spectra were collected on a Shimadzu FTIR-8400S spectrometer using KBr disks. Thermogravimetric analyses (TGA) were performed in air (100 mL/min) at the heating rate of 5 °C/min from 293 to 1173 K using a Mettler Toledo TGA/SDTA 851e analyzer. Powder X-ray diffraction patterns were recorded on a Philips X'Pert counter diffractometer working with Cu K_α radiation and operating over the temperature range (293−380 K). The heating/cooling rate was 10 K/minute between two steps of analysis. Indexation of unit cell parameters was carried out using the DICVOL04 software.[52] DSC measurements were carried out in a $He_{(g)}$ atmosphere using a Perkin-Elmer DSC Pyris 1 instrument equipped with a cryostat and operating down to 98 K. An aluminum capsule was loaded with 30.4 mg of sample and hermetically sealed. The heating and cooling rates were fixed at 10 K/minute. Temperatures and enthalpies were calibrated over the temperature range of interest using the solid−liquid transitions of pure Indium (99.99%).[39] The sample was maintained at room temperature for 5 min to allow the system to equilibrate, and was further warmed from 293 to 400 K. The sample was maintained at the highest temperature for 5−10 min to reach equilibrium, followed by a similar scanning mode as on warming, between 400 K and room temperature. The experiment was carried out 4 times to check the reproducibility. Scanning electron microscopy (SEM) was performed using a Gemini Digital Scanning Microscope 982 with 1 kV accelerating voltage with an aluminum sample holder. Diffuse reflectance spectra were obtained with a Varian Cary 5E spectrophotometer using PTFE as a reference. Measurements at 400 K were carried out using a homemade heating procedure. ^{57}Fe Mössbauer spectra were recorded in transmission geometry over the temperature range 293−380 K with a WissEL spectrometer equipped with a Cyclotron ^{57}Co(Rh) radioactive source. The sample was sealed in aluminum foil and mounted on an oven equipped with a WEST 3810 temperature controller. The spectra were fitted to the sum of Lorentzians by a least-squares refinement using Recoil 1.05 Mössbauer Analysis Software.[53] All isomer shifts refer to α-Fe at room temperature. Debye−Waller factors for HS and LS Fe^{II} ions were assumed as equal. This way, the HS molar fraction was directly derived from the relative area fraction. Magnetic susceptibilities were measured in the temperature range 269−380 K using a MPMS-XL (7T) SQUID magnetometer. Data were corrected for magnetization of the sample holder and diamagnetic contributions, which were estimated from the Pascal constants. The FORC distribution is determined at each point by fitting a mixed second-order polynomial of the form $[a_1 + a_2T_a + a_3T_b + a_4T_a^2 + a_5T_b^2 + a_6T_aT_b]$ to a local moving grid. When interpolation is done to obtain the distribution value we take into consideration also the neighboring interpolated point. In this case the value of $-a_6$ provides the mixed second derivative of the fitted surface, and it can be assigned to the center of the grid as a representation of the density of the FORC distribution $\rho(T_a,T_b)$ at that point. The value of the magnetization is interpolated in every measured point with that polynomial of second order.

Single Crystal X-ray Diffraction. A blue crystal of **2** was selected and mounted with epoxy glue on a glass capillary. The measurement was carried out at 293 K using an Oxford Diffraction Xcalibur 2 diffractometer with Mo K_α radiation. The exposure time was 10 s per frame and the crystal-detector distance was 60 mm. Data reduction and analytical absorption correction were performed using the CRYSALIS RED software suite.[54] The final lattice parameters (a = 16.635(6) Å, b = 13.223(4) Å, c = 7.805(3) Å, β = 102.56(3)°) were calculated from all reflections observed in the actual data collection. Systematic absences indicated the monoclinic space group $C2/c$. The structure was solved by direct methods using SIR 2004,[55] which revealed the atomic positions, and refined by using the SHELX-97 program package.[56] The final refinements were carried out on F_o^2. Atomic scattering factors for spherical neutral free atoms were taken from standard sources, and anomalous dispersion

(52) Boultif, A.; Louër, D. *J. Appl. Crystallogr.* **2004**, *37*, 724.

(53) Lagarec, K.; Rancourt, D. G. *Recoil Mössbauer Spectral Analysis Software for Windows 1.0*; Department of Physics, University of Ottawa: Canada, 1998.

(54) Oxford Diffraction. *CRYSALIS RED*, v.1.71; Oxford Diffraction Ltd.: Oxford, U.K., 2004.

(55) Burla, M. C.; Caliandro, R.; Camalli, M.; Carrozzini, B.; Cascarano, G. L.; De Caro, L.; Giacovazzo, C.; Polidori, G.; Spagna, R. *J. Appl. Crystallogr.* **2005**, *38*, 381.

(56) Sheldrick, G. M. *SHELXL-97: Program for crystal structure refinement*; University of Göttingen: Göttingen, Germany, 1997.

corrections were applied.[57] Final R indices were $R_1 = 0.0534$, $wR_2 = 0.1423$ for $[I > 2\sigma(I)]$ and $R_1 = 0.0614$, $wR_2 = 0.1510$ for all data.

Acknowledgment. This work was partly funded by the IAP VI (P6/17) INANOMAT, the FNRS-FRFC (No 2.4508308), a Concerted Research Action of the "Communauté Française de Belgique" allotted by the Académie Universitaire Louvain and a DARPA Grant HR0011-07-1-0031.

(57) Cromer, D. T.; Waber, J. T. *International Tables for X-ray Crystallography 4*; Kynoch Press: Birmingham, England, 1974; Table 2.2 A and Table 2.3.1.

Supporting Information Available: TGA of **1** and CIF file for **2**. This material is available free of charge via the Internet at http://pubs.acs.org.